JPE 16-3-40

http://dx.doi.org/10.6113/JPE.2016.16.3.1236
ISSN(Print): 1598-2092 / ISSN(Online): 2093-4718

Design and Implementation of an Active EMI Filter for Common-Mode Noise Reduction

Kuk-Hee Lee*, Byeong-Geuk Kang*, Yongoh Choi*, Se-Kyo Chung†,
Jae-Sun Won**, and Hee-Seung Kim**

*, †Department of Control and Instrumentation Engineering, Gyeongsang National University, Jinju, Korea
**Wireless Power Transfer Team, Samsung Electro-Mechanics, Suwon, Korea

Abstract

This paper presents the analysis and design of an active electromagnetic interference (EMI) filter (AEF) for the common-mode (CM) noise reduction of switching power converters. The features of the several types of AEFs are discussed and compared in terms of implementation. The feed-forward AEF with a voltage-sensing and voltage-cancellation (VSVC) structure is implemented for an LLC resonant converter to replace a multiple-stage passive EMI filter and thereby reduce CM noise. The characteristics and performance of the VSVC-type AEF are investigated through theoretical and experimental works.

Key words: Active EMI filter, Common-mode noise, EMI, Noise reduction

I. INTRODUCTION

The reduction of electromagnetic interference (EMI) is a significant issue in the design and implementation of high-power density switching power converters. A power-line EMI filter is a traditional solution to reduce the conducted emissions of converters [1]. A passive filter with a common-mode (CM) choke and X and Y capacitors is generally used for this purpose. However, this filter is bulky, and the manufacturing of the filter components, such as the CM choke, is too laborious.

In recent years, active EMI filters (AEFs) have been considered as an alternative to passive filters. AEFs perform an active cancellation of noise instead of LC filtering. Hence, they do not require bulky passive components. Moreover, they show great potential for integration into EMI filters in a small chip or package.

Research on AEF can be found in the literature [2]-[10]. The active cancellation of noise currents using AEFs was studied in [2]-[7]. Voltage cancellation and hybrid methods were reported in [8]-[10]. Differential mode (DM) AEFs were also considered in [5], [10]. Despite the extensive study on the usefulness of AEFs, further research on AEF circuits and components should still be performed for practical design and implementation.

This paper presents the design and implementation of active EMI filters for the CM noise reduction of LLC resonant converters. The characteristics of several AEF topologies are discussed and compared. The control loop characteristics of feedback and feed-forward AEFs are also investigated. A feed-forward AEF with a voltage-sensing and voltage-cancellation (VSVC) structure is finally implemented to replace the multiple-stage passive EMI filter. The performance of the implemented AEF in terms of EMI reduction is investigated through experimental works.

II. STRUCTURE OF ACTIVE EMI FILTER

A. Active EMI Filter Topologies

Fig. 1 shows the structure of the AEF for the CM noise reduction of switching power converters. The conducted noise of the power line is measured and is actively cancelled by the compensating voltage or current generated from the control amplifier.

Four types of AEF topologies can be considered for the combination of the sensing and cancellation methods. The simplified CM equivalent circuits of four AEF types are shown in Fig. 2. In terms of implementation, voltage sensing

Manuscript received Dec. 9, 2015; accepted Mar. 3, 2016
Recommended for publication by Associate Editor Lixiang Wei.
†Corresponding Author: skchung@gnu.ac.kr
Tel: +82-55-772-1744, Fax: +82-55-772-1749, Gyeongsang Nat'l Univ.
*Dept. of Control and Instrumentation Eng., Gyeongsang National University, Korea
**Wireless Power Transfer Team, Samsung Electro-Mechanics, Korea

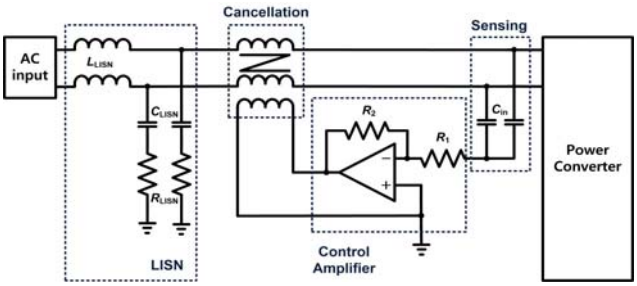

Fig. 1. Structure of active EMI filter for CM noise reduction.

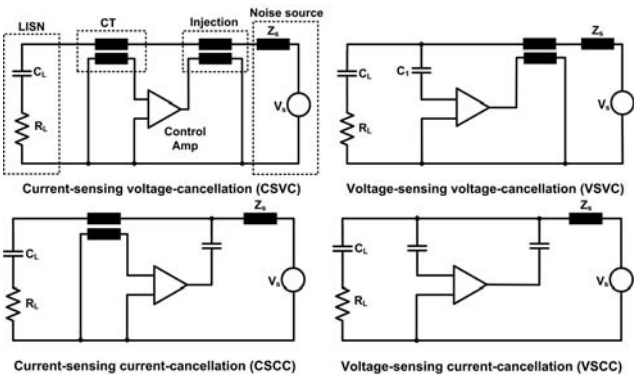

Fig. 2. Types of AEFs.

is simpler than current sensing because it does not require a current transformer. Meanwhile, the current capability of control amplifiers is crucial for the selection of a cancellation method. The current type is difficult to implement because of the lack of a high-current and wide-bandwidth operational amplifier (OP amp). The possibility of a high CM current occurring is another problem for this method because it makes a bypassing path to the ground. As a result, the VSVC type is considered for the implementation of the AEF in this study.

B. Characteristics of Feedback and Feed-forward AEFs

In view of the control loop, two AEF structures can be considered according to the point of the measurement of noise signals. A noise signal is measured at the LISN terminals (control target) in the feedback control and at the converter input (noise source) in the feed-forward control.

Fig. 3 shows the CM equivalent circuits of the VSVC-type feedback and feed-forward AEFs. The transfer functions of both AEFs are derived to investigate the characteristics of the control loops. The transfer function of the feedback AEF is given as

$$\frac{V_o}{V_s} = \frac{R_L}{Z_S + (1+A)Z_L} \tag{1}$$

where V_s, V_o, Z_s, R_L, and A denote the voltage of the noise source, voltage of the LISN terminal, noise source impedance, resistance of the LISN, and forward gain of the control loop, respectively. The measurement of noise source impedance is discussed in [11]. The total impedance Z_L of the LISN side can be represented as

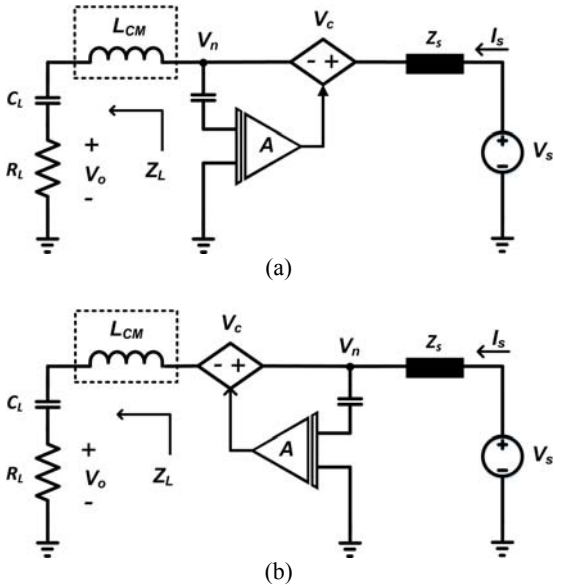

Fig. 3. CM equivalent circuit of feedback and feed-forward AEFs. (a) Feedback AEF (b) Feed-forward AEF.

$$Z_L = \frac{1}{sC_L} + R_L \tag{2}$$

or

$$Z_L = sL_{CM} + \frac{1}{sC_L} + R_L \tag{3}$$

for the circuits with or without the additional CM choke, respectively, where L_{CM} is the inductance of the additional CM choke. The small CM choke is generally combined to reduce the EMI in the high frequency range over few tens MHz because of the frequency limitation of the filter components, such as the OP amp and injection transformer.

The transfer function of the feed-forward AEF can also be derived from Fig. 3(b) as

$$\frac{V_o}{V_s} = \frac{(1-A)R_L}{(1-A)Z_S + Z_L} \tag{4}$$

As indicated in (1), an extremely high value of the forward gain A is required to minimize the noise voltage (V_o) at the LISN terminal for the feedback AEF. However, the noise voltage tends to drop to zero as the forward gain A approaches unity (A = 1) for the feed-forward AEF, as shown in (4). Therefore, the feed-forward structure is chosen for the implementation.

III. DESIGN AND IMPLEMENTATION

The CM circuit diagram of the VSVC type feed-forward AEF is shown in Fig. 4. The diagram consists of a sensing circuit, a control amplifier, and a voltage injection transformer. The forward gain A can be represented as follows using the three blocks:

$$A(s) = G_T(s)G_c(s)H_s(s) \tag{5}$$

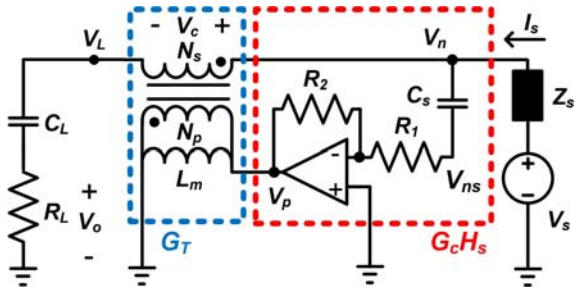

Fig. 4. CM circuit of VSVC-type feed-forward AEF.

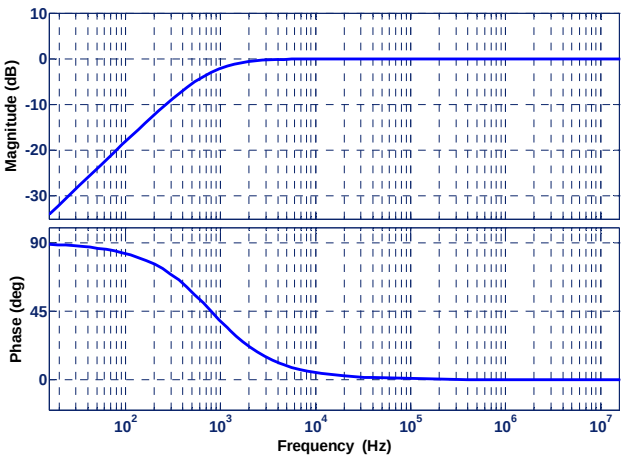

Fig. 5. Simulated frequency response of sensing circuit ($R_1 = 10\ k\Omega$, $C_s = 20\ nF$ and $f_h = 796\ Hz$).

where G_T, G_c, and H_s are the transfer functions of the injection transformer, control amplifier, and sensing circuit, respectively. The characteristics and design of each part are discussed in the next section.

A. Sensing Circuit

The sensing circuit in Fig. 4 is a first-order high-pass filter. The transfer function of this circuit can be given as follows using the concept of virtual ground:

$$H_s(s) = \frac{V_{ns}}{V_n} = \frac{s}{s + \frac{1}{R_1 C_s}} \tag{6}$$

Its cut-off frequency is given as $f_h = 1/(2\pi R_1 C_s)$. The cut-off frequency of the sensing circuit should be lower than the lowest frequency component of the noise voltage. It is thus determined to be the value that is sufficiently lower than the lowest switching frequency f_s of the LLC resonant converter ($f_s = 80kHz$ in this design). Fig. 5 shows the simulated result for the frequency response of the sensing circuit, where $R_1 = 10k\Omega$, $C_s = 20nF$, and $f_h = 796Hz$.

B. Control Amplifier

The OP amp is generally used for a control amplifier that generates a cancellation voltage. The gain of the inverting amplifier shown in Fig. 4 can be represented as

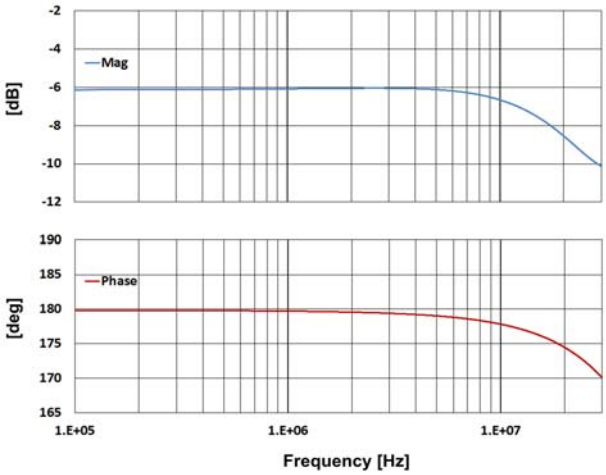

Fig. 6. Measured gain/phase response $G_c(s)$ of inverting amplifier using OPA847 ($R_1 = 10k\Omega$, $R_2 = 5k\Omega$).

TABLE I
OP AMP SPECIFICATIONS (OPA847)

Item	Value
Gain bandwidth product (GBP)	3.9 GHz
Slew rate	950 V/us
Maximum output voltage swing ($V_{op,max}$)	+/−5V
Maximum output current ($I_{op,\ max}$)	
- Source	100 mA
- Sink	−75 mA

$$G_c(s) = \frac{V_p}{V_{ns}} = -\frac{R_2}{R_1}\frac{\omega_c}{s + \omega_c} \tag{7}$$

where R_1, R_2, and ω_c ($= 2\pi f_c$) are the feedback resistor, input resistor, and −3 dB frequency of the OP amp, respectively. The phase response of the OP amp circuit is more important than the gain because the phase delay of the control amplifier severely degrades the performance of the feed-forward AEF, especially in the high frequency range. In the worst case, a large phase delay may amplify the noise by summing up the noise and cancellation voltages. Fig. 6 shows the measured gain/phase responses of the inverting amplifier using the OP amp OPA847, where $f_c = 22MHz$. Several important parameters of OPA847 are summarized in Table 1. The frequency response of the OP amp in the low gain ($|G_c| < 1$) is important for the high frequency range, but it is not a major concern in practice because the injection transformer exhibits a relatively slow response, which is dominant in the control loop.

The output voltage swing and current capability of the OP amp are critical parameters in real implementation. The OP amp should supply sufficient current to magnetize the injection transformer, and the input voltage of the transformer should be within the maximum output voltage swing $V_{op,max}$. These requirements are discussed in the next section.

C. Injection Transformer

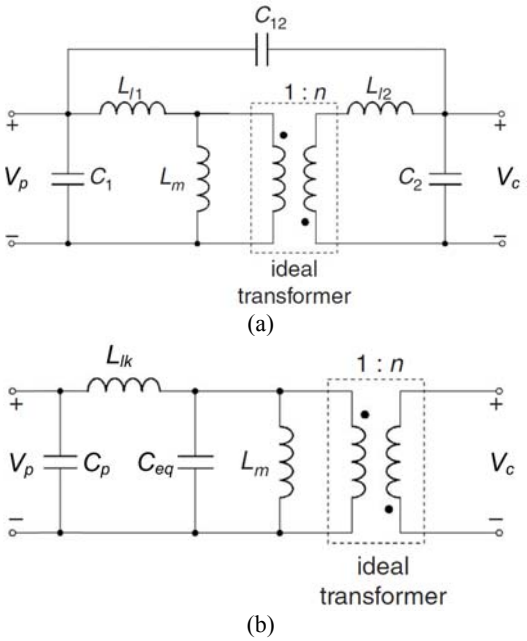

Fig. 7. Circuit model of injection transformer. (a) CM equivalent circuit model. (b) Simplified model.

The output voltage of the OP amp is applied to the primary terminal of the transformer, and the CM noise voltage V_n can be canceled by the secondary voltage V_c connected in series to the CM path. The CM equivalent circuit of the transformer is shown in Fig. 7(a); its simplified form is shown in Fig. 7(b) [12], where

$$C_p = C_1 + (1-n)C_{12} \tag{8}$$

$$C_{eq} = n^2\left[C_2 + \left(1-\frac{1}{n}\right)C_{12}\right] \tag{9}$$

$$L_{lk} = L_{l1} + \frac{1}{n^2}L_{l2} \tag{10}$$

and $n = N_s / N_p$. The symbols C_1, C_2, C_{12}, L_{l1}, L_{l2}, and L_m denote the capacitance of the primary terminal, capacitance of the secondary terminal, inter-winding capacitance, leakage inductance of the primary winding, leakage inductance of the secondary winding, and magnetizing inductance, respectively.

The transfer function of the injection transformer can be derived from Fig. 7(b) and for $L_m \gg L_{lk}$ as

$$G_T(s) = \frac{V_s}{V_p} = n\left(\frac{L_m}{L_m + L_{lk}}\right)\left(\frac{\omega_T^2}{s^2+\omega_T^2}\right) \simeq n\left(\frac{\omega_T^2}{s^2+\omega_T^2}\right) \tag{11}$$

where

$$\omega_T = \frac{1}{\sqrt{(L_{lk} \parallel L_m)C_{eq}}} \simeq \frac{1}{\sqrt{L_{lk}C_{eq}}} \tag{12}$$

As shown in (11) and (12), the leakage inductance L_{lk} and equivalent winding capacitance C_{eq} are the parameters that determine the bandwidth of the injection transformer. Thus, these parameters should be minimized to reduce high frequency noise.

TABLE II
PARAMETERS OF IMPLEMENTED TRANSFORMER

Item	Value
Core material	Nanocrystalline
Permeability of core (μ_r)	14,000
Inductance constant (A_L)	8 uH/turn^2
Cross-sectional area of core (A_c)	0.19 cm^2
Mean length of core (l_e)	4.08 cm
Turns ratio (n=N_s/N_p)	2 (4:8)
Magnetizing inductance (L_m)	213 uH
Leakage inductance (L_{lk})	2.72 uH
Equivalent winding capacitance (C_{eq})	79 pF

The maximum output voltage swing and current capability of the OP amp should also be considered in the transformer design. The peak value of the primary voltage $V_{p,\,peak}$ should be within the maximum output swing $V_{op,\max}$ of the OP amp; that is,

$$V_{p,peak} \simeq \frac{1}{n}V_{s,peak} < V_{op,\max} \tag{13}$$

where $V_{s,peak}$ denotes the peak voltage of the transformer output. The input current of the transformer is also limited by the maximum output current $I_{op,\max}$ of the OP amp, as shown in (14).

$$I_{p,peak} = \frac{V_{p,peak}}{|Z_{Ti}|} < I_{op,\max} \tag{14}$$

where Z_{Ti} denotes the input impedance of the transformer. The primary turns of the transformer can be determined as

$$N_p = \sqrt{\frac{L_m}{A_L}} \tag{15}$$

where

$$A_L = \frac{\mu_0\mu_r A_c}{l_c} \tag{16}$$

and μ_0, μ_r, A_c, and l_c denote air permeability, relative permeability, cross-sectional area, and mean length of the magnetic core, respectively.

The selection of core materials is extremely important in miniaturizing transformer size and improving high frequency characteristics. The large number of turns of the transformer winding increases the leakage inductance and winding capacitance, which in turn degrade the frequency response. Hence, the core material should exhibit high permeability to reduce winding turns. A nanocrystalline core with $\mu_r = 14{,}000$ is used for the implementation. The parameters of the implemented injection transformer are listed in Table II.

Fig. 8 shows the measured gain/phase response $G_T(s)$ of the injection transformer, the poles of which are located at 10.9

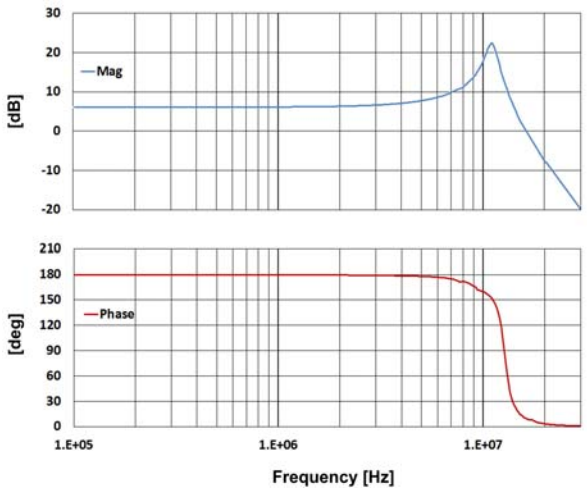

Fig. 8. Measured gain/phase response of the transformer $G_T(s)$.

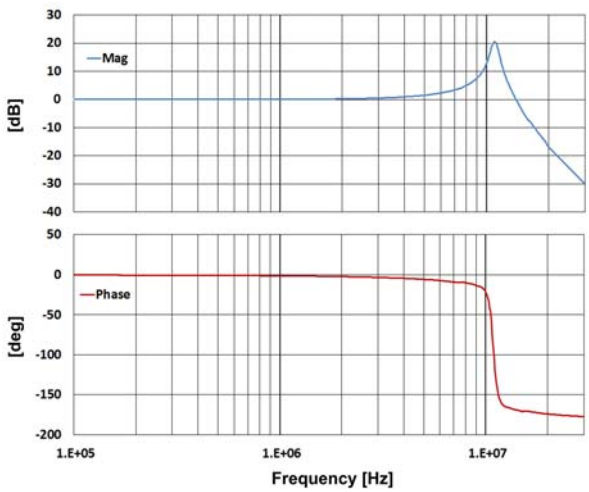

Fig. 9. Measured gain/phase response of the OP amp and transformer $G_c(s)G_T(s)$.

MHz. The measured total response $G_c(s)G_T(s)$, including the OP amp and transformer, is shown in Fig. 9. Both figures show that the frequency response of the control loop is governed by the transformer characteristics.

D. Discussion on Stability

The feed-forward AEF does not have any feedback signals in the control loop. However, we note that in (4), the natural feedback loop is made by the impedance of the noise source Z_s. We can rewrite (4) for the voltage V_L shown in Fig. 4 as

$$\frac{V_L}{V_s} = \frac{(1-A)}{1+(1-A)\dfrac{Z_s}{Z_L}} \tag{17}$$

If the source impedance $Z_s = 0$, then the transfer function is $(1 - A)$, and only the feed-forward loop exists. However, for the case in which $Z_s \neq 0$, a feedback loop is made with the forward and feedback gains of $(1 - A)$ and Z_s/Z_L, respectively. Consequently, the operation of the AEF becomes unstable for a certain condition of gain A.

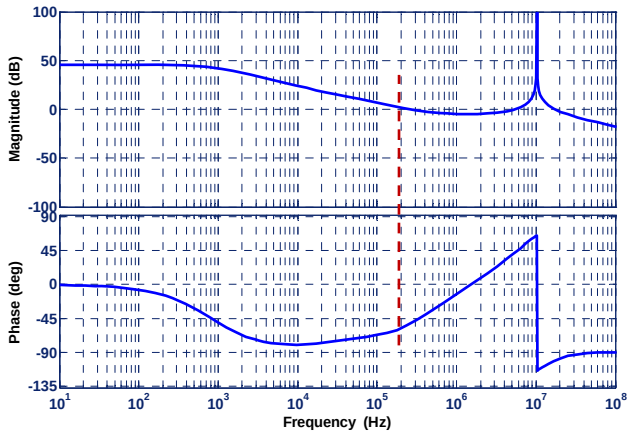

Fig. 10. Bode plot of loop gain $(1 - A)Z_s/Z_L$ for $n(R_2/R_1) = 0.98$.

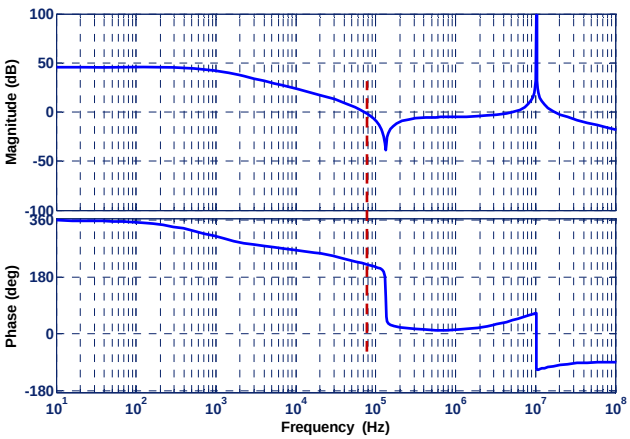

Fig. 11. Bode plot of loop gain $(1 - A)Z_s/Z_L$ for $n(R_2/R_1) = 1$.

Figs. 10 and 11 show the Bode diagrams of the loop gain $(1 - A)\cdot Z_s/Z_L$ for the DC gain of $G_c(s)G_T(s)$, $(R_2/R_1)\cdot n = 0.98$ and 1, respectively, where $Z_s = 1/\,j(2\pi f \cdot 1nF)$, $C_L = 0.1$ uF, and $R_L = 50\ \Omega$. As shown in Fig. 10, the gain and phase margins are sufficient, and the feedback loop is stable. However, these margins decline rapidly for $(R_2/R_1)\cdot n = 1$, as shown in Fig. 11. Therefore, this condition should be avoided for the stable operation of the feed-forward AEF.

IV. Experimental Results and Discussion

Figs. 12 and 13 show the implemented AEF and experimental setup, respectively. The LLC resonant converter with a power rating of 500 W is used for the test, in which the AEF replaces the three-stage passive CM filter. The tested conditions are given in Table III.

Fig. 14 shows the CM noise spectrum without any EMI filter, with the reference line being the EN55022 limit. The CM noise is severe in the frequency range of 150 kHz to 3 MHz. The CM noise spectrum with the three-stage passive filter is shown in Fig. 15, in which the CM noise is below the limit line.

Fig. 16 shows the experimental waveforms of the AEF and CM noise spectrum for $(R_2/R_1)\cdot n = 1$, where $R_1 = 10k\Omega$ and

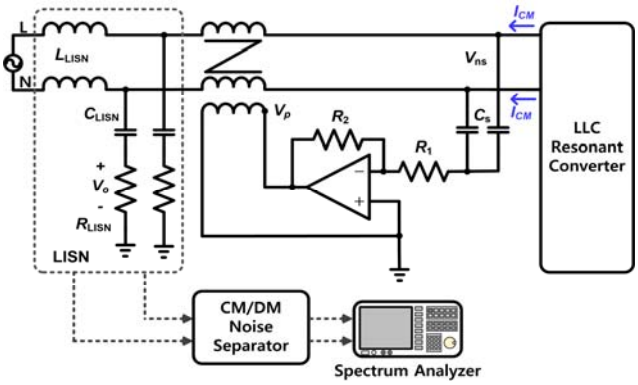

Fig. 12. Experimental setup.

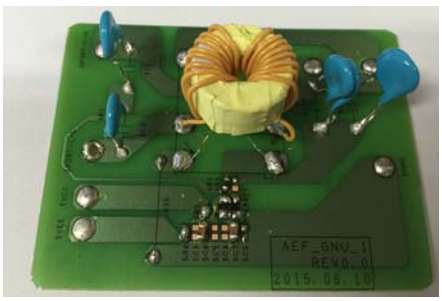

Fig. 13. Photograph of implemented AEF.

TABLE III
EXPERIMENTAL CONDITIONS

Item	Value
Power rating of tested converter	500 W
Switching frequency of tested converter (f_s)	80–120 kHz
Input voltage	220 Vac
Capacitance of LISN (C_L)	0.1 uF
Resistance of LISN (R_L)	50 Ω

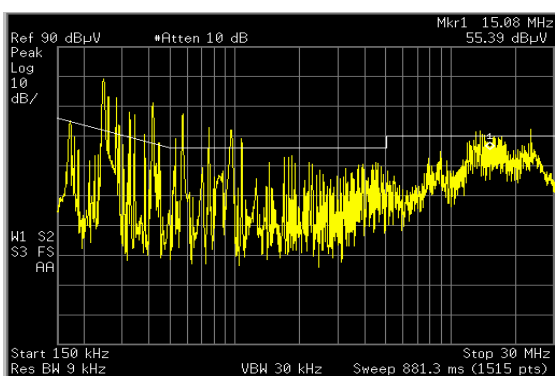

Fig. 14. CM noise spectrum without an EMI filter.

$R_2 = 5k\Omega$. As shown in Fig. 16(a), the output voltage V_{op} of the OP amp is saturated to $V_{op,max}$ and cannot fully cancel the noise voltage. The low frequency spectrum exceeds the desired EMI limit, as shown in Fig. 16(b). As discussed in the previous section, the feedback loop is unstable for this condition, and the output voltage of the OP amp is saturated. This problem can be solved by applying the slightly reduced OP amp gain.

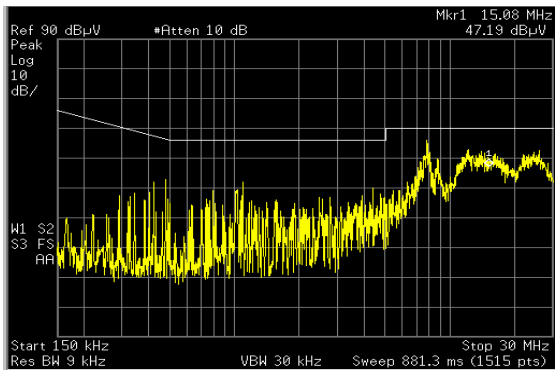

Fig. 15. CM noise spectrum with a three-stage passive EMI filter.

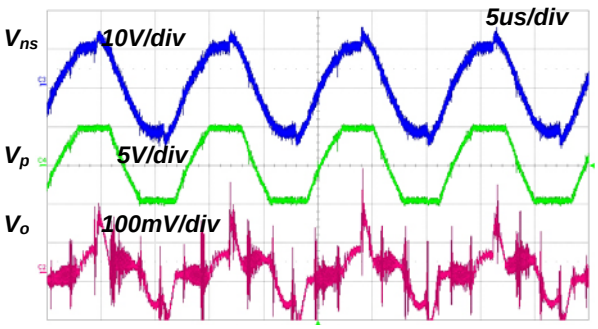

(a)

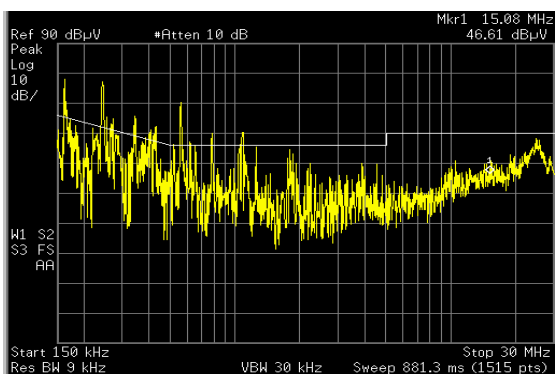

(b)

Fig. 16. Experimental results for $(R_2/R_1)\cdot n = 1$, $R_1 = 10k\Omega$, and $R_2 = 5k\Omega$. (a) Experimental waveforms of AEF. (b) CM noise spectrum.

Fig. 17 shows the experimental results for $(R_2/R_1)\cdot n = 0.97$, where $R_1 = 10.3k\Omega$ and $R_2 = 5k\Omega$. The figure clearly shows the significant improvement in the EMI performance. The peak output voltage of the OP amp is within the maximum voltage swing $V_{op,max}$, and the sensed noise voltage V_{ns} and OP amp output V_{op} exhibit nearly the same shape, as shown in Fig. 17(a). Thus, the CM noise voltage is successfully canceled, and an extremely small LISN voltage V_o is observed. The CM noise spectrum for this condition is shown in Fig. 17(b). The noise margin of over 10 dB for the EN55022 limit line can be obtained for the frequency range of 150 kHz–20 MHz. As predicted in the frequency response of $G_c(s)G_I(s)$ shown in Fig. 10, the AEF performance declines at a frequency of over 15

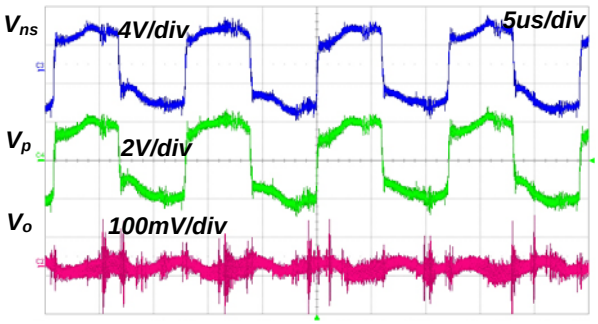

(a)

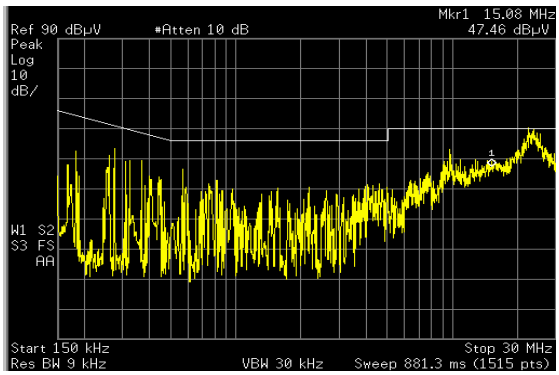

(b)

Fig. 17. Experimental results for $(R_2/R_1)\cdot n = 1$, $R_1 = 10.3k\Omega$, and $R_2 = 5k\Omega$. (a) Experimental waveforms of AEF. (b) CM noise spectrum.

MHz because of the limited bandwidth of the injection transformer. In the frequency range below 20 MHz, the performance of the implemented AEF is comparable to that of the three-stage passive filter shown in Fig. 15. A noise voltage above this range can be reduced by employing a small high-frequency CM choke.

V. CONCLUSIONS

This study presented the design and implementation of an AEF for the CM noise reduction of switching power converters. A VSVC-type feed-forward AEF was considered for the implementation and used to replace the three-stage passive EMI filter. The practical considerations for the implementation of the filter were provided. Such considerations include the output voltage swing and current capability of the OP amp, the frequency characteristics of the filter components, and the stability of the feed-forward AEF. The operation and performance of the implemented AEF were investigated through the experimental works for an LLC resonant converter with a power rating of 500 W. The experimental results show that a noise margin of over 10 dB for the EN55022 limit can be obtained for the frequency range of 150 kHz–20 MHz by employing the implemented AEF. The designed AEF can replace bulky passive filters and be successfully used to reduce low-frequency EMI.

APPENDIX

Equations (1) to (4) can be derived as follows. The voltage equation of the CM loop for the feedback AEF can be represented in Fig. 3(a) as

$$V_s = Z_s I_s + V_c + V_n \tag{18}$$

The output voltage of the injection transformer and the voltage of the sensing point are respectively given as

$$V_c = AV_n \tag{19}$$

$$V_n = Z_L I_s \tag{20}$$

where the current flowing from the sensing point to the control amplifier is neglected; the equivalent impedance Z_L is shown in (2) and (3) in Section II-B. The LISN terminal voltage is represented as

$$V_o = I_s R_L \tag{21}$$

and the transfer function can be derived from (18) to (21) as

$$\frac{V_o}{V_s} = \frac{R_L}{Z_s + (1+A)Z_L}. \tag{22}$$

The voltage equation of the CM loop for the feed-forward AEF can also be represented in Fig. 3(b) as

$$V_s = Z_s I_s + V_c + Z_L I_s \tag{23}$$

where

$$V_c = AV_n \tag{24}$$

$$V_n = V_s - Z_s I_s \tag{25}$$

The LISN terminal voltage is also represented as

$$V_o = I_s R_L \tag{26}$$

and the transfer function can be derived from (23) to (26) as

$$\frac{V_o}{V_s} = \frac{(1-A)R_L}{(1-A)Z_s + Z_L}. \tag{27}$$

REFERENCES

[1] F. Costa, C. Gautier, E. Laboure, and B. Revol, *Electromagnetic Compatibility in Power Electronics*, ISTE Ltd and John Wiley & Sons, Inc. 2014.

[2] Y. C. Son and S. K. Sul, "A new active common-mode EMI filter for PWM inverter," *IEEE Trans. Power Electron.*, Vol. 18, No. 6, pp. 1309-1314, Nov. 2003.

[3] C. Wenjie, Y. Xu, and W. Zhaoan, "Design and evaluation of an input active EMI filter for integrated power electronics modules," in *IEEE 36th Power Electronics Specailists Conference*, pp. 309-312, Jun. 2005.

[4] W. Chen, X. Yang, and Z. Wang, "An active EMI filtering technique for improving passive filter low-frequency performance," *IEEE Trans. Electromagn. Compat.*, Vol. 48, No. 1, pp. 172-177, Feb. 2006.

[5] W. Chen, W. Zhang, X. Yang, and Z. Sheng, "An experimental study of common- and differential-mode active EMI filter compensation characteristics," *IEEE*

Trans. Electromagn. Compat., Vol. 51, No. 3, pp. 683-691, Aug. 2009.
[6] M. L. Heldwein, H. Ertl, J. Biela, and J. W. Kolar, "Implementation of a transformerless common-mode active filter for offline converter systems," *IEEE Trans. Ind. Electron*., Vol. 57, No. 5, pp. 1772-1786, May 2010.
[7] Z. Rong, F. Panlong, D. Wei, and X. Rui, "Design of active EMI filter based on virtual impedance transform method," in *2nd International Symposium on Instrumentation and Measurement, Sensor Network and Automation (IMSNA)*, pp. 871-874, Dec. 2013.
[8] D. Hamza and P. K. Jain, "Conducted EMI noise mitigation in DC-DC converters using active filtering method," in *IEEE Power Electronics Specialists Conference*, pp. 188-194, Jun. 2008.
[9] D. Hamza, M. Sawan, and P. K. Jain, "Suppression of common-mode input electromagnetic interference noise in DC–DC converters using the active filtering method," *IET Power Electronics*, Vol. 4, No. 7, pp. 776–784, Aug. 2011.
[10] M. Ali, E. Labour´e, and F. Costa, "Integrated active filter for differential-mode noise suppression," *IEEE Trans. Power Electron*., Vol. 29, No. 3, pp. 1053-1057, Mar. 2014.
[11] K. Y. See and J. Deng, "Measurement of noise sourceimpedance of SMPS using a two probes approach," *IEEE Trans. Power Electron.*, Vol. 19, No. 3, pp. 862–868, May 2004.
[12] U. A. Bakshi and M. V. Bakshi, *Magnetic Circuits and Transformer*, 1st Edition, Technical Publications Pune, 2008.
[13] C. T. McLyman, *Transformer and Inductor Design Handbook 3rd Edition*, Marcel Dekker, 2004.

Kuk-Hee Lee was born in Busan, Korea, in 1992. She received her B.S. and M.S. degrees in Control and Instrumentation Engineering from Gyeongsang National University, Jinju, Korea, in 2014 and 2016, respectively. Her research interests include switching power converters and magnetic design.

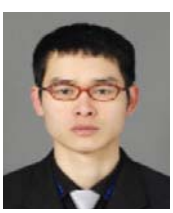

Byeong-Geuk Kang was born in Hapcheon, Korea, in 1983. He received his B.S. and M.S. degrees in Control and Instrumentation Engineering from Gyeongsang National University, Jinju, Korea, in 2008 and 2010 respectively. He is now working toward his Ph.D. degree at the same university. His research interests include switching power converters and magnetic design.

Yongoh Choi was born in Miryang, Korea, in 1986. He received his B.S. and M.S. degrees in Control and Instrumentation Engineering from Gyeonsang National University, Jinju, Korea, in 2011 and 2014, respectively. His research interests include switching power converters and wireless power transform.

Se-Kyo Chung was born in Daegu, Korea, in 1966. He received his B.S. degree in Electronic Engineering from Kyungpook National University, Daegu, in 1989, and his M.S. and Ph.D. degrees in Electrical Engineering from the Korea Advanced Institute of Science and Technology (KAIST), Daejeon, in 1992 and 1997, respectively. Since 1997, he has been with the Department of Control and Instrumentation Engineering, Gyeongsang National University, Jinju, Korea, where he is a Professor and Principal Researcher of the Engineering Research Institute. He was a Visiting Professor of Electric Power Control Lab, Kyushu Institute of Technology, Kitakyushu, Japan, in 2000, and a Visiting Scholar at Texas A&M University, College Station, TX, USA, in 2002 and 2012. His research interests lie in the areas of power electronics and control, which include high-performance ac machine drives, switching power converters, magnetic design, and power electronics interface to micro-grids. Dr. Chung is an Associate Editor of Journal of Power Electronics.

Jae-Sun Won was born in Wonju, Korea, in 1973. He received his M.E. and Ph.D. degrees in Electrical Engineering from Yeungnam University, Gyeongsan, Korea, in 1999 and 2005, respectively. He is currently working with the Wireless Power Transfer (WPT) Team of the Digital Module Division of Samsung Electro-Mechanics, Suwon, Korea, as a Principal Engineer. His research interests include resonant inverter/converter systems, soft switching technology, electromagnetic interference (EMI) design of power electronics, and wireless power transfer systems.

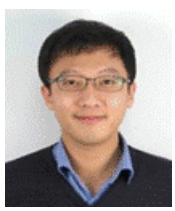

Hee-Seung Kim was born in Seoul, Korea, in 1982. He received his B.S., M.S., and Ph.D. degrees in Electronic Engineering from Kookmin University, Seoul, Korea, in 2008, 2010, and 2013, respectively. He is currently working with the Wireless Power Transfer (WPT) Team of the Digital Module Division of Samsung Electro-Mechanics, Suwon, Korea, as a Senior Engineer. His research interests include magnetic devices, electromagnetics analysis, power conversion system design, electromagnetic interference (EMI) design of power electronics, and wireless power transfer systems.